In Situ Transmission Electron Microscopy Observation of Nanostructural Changes in Phase-Change Memory

Stefan Meister,[†] SangBum Kim,[‡] Judy J. Cha,[†] H.-S. Philip Wong,[‡] and Yi Cui[†,*]

[†]Department of Materials Science and Engineering, Stanford University, Stanford, California 94305, United States, and [‡]Department of Electrical Engineering, Stanford University, Stanford, California 94305, United States

ABSTRACT Phase-change memory (PCM) has been researched extensively as a promising alternative to flash memory. Important studies have focused on its scalability, switching speed, endurance, and new materials. Still, reliability issues and inconsistent switching in PCM devices motivate the need to further study its fundamental properties. However, many investigations treat PCM cells as black boxes; nanostructural changes inside the devices remain hidden. Here, using *in situ* transmission electron microscopy, we observe real-time nanostructural changes in lateral $Ge_2Sb_2Te_5$ (GST) PCM bridges during switching. We find that PCM devices with similar resistances can exhibit distinct threshold switching behaviors due to the different initial distribution of nanocrystalline and amorphous domains, explaining variability of switching behaviors of PCM cells in the literature. Our findings show a direct correlation between nanostructure and switching behavior, providing important guidelines in the design and operation of future PCM devices with improved endurance and lower variability.

KEYWORDS: data storage · characterization tools · nanostructures · thin films

Phase-change memory (PCM) uses the large difference in resistivity between crystalline and amorphous phases of chalcogenide glasses to store information.[1] Switching between the two phases is accomplished via Joule heating by a voltage pulse. In order to switch from the stable crystalline phase to the metastable amorphous phase, the material is melted and rapidly quenched, freezing the atoms in place before they have time to recrystallize. For the reverse transformation, from amorphous to crystalline, the material is heated above its crystallization temperature for a sufficient time. Despite the high resistivity of the amorphous phase, crystallization can be achieved by a relatively small voltage pulse because PCM materials exhibit threshold switching.[2−4] Threshold switching occurs when a critical electric field is applied across the amorphous region, resulting in conductive filaments that can facilitate sufficient heating to induce crystallization. Recent work by Ielmini describes how this conductive filament can form through hopping mechanisms of electrons, initiated by the applied electric field, in chalcogenide glasses.[5]

Important studies in PCM have focused on its scalability,[6−11] switching speed,[10,12,13] endurance,[8,10,13] and new materials.[10,12−15] Still, reliability issues and inconsistent switching in PCM devices motivate the need to further study the relationship between the nanostructure and electrical behavior. While the atomistic mechanisms involved in the phase transition have been studied in great detail,[16−21] few experiments show what the nanostructures of the amorphous or crystalline regions look like before and after switching. However, knowing the detailed nanostructure is important because it relates directly to electrical properties such as the electric field required to induce threshold switching, sources of variability in switching, or the origin of resistance drift.[22,23] Fluctuation microscopy has been used to characterize medium- and long-range orders of the glassy state of the thermally treated chalcogenide films.[24,25] Moreover in an effort to study the nanostructure changes during the PCM operation, researchers have obtained transmission electron microscopy (TEM) images by cutting individual PCM cells out of a chip with a focused ion beam.[26,27] This technique provides a snapshot in time of individual cells, but it does not allow for a direct correlation between nanostructure and electrical behavior during repeated switching. A variety of *in situ* TEM techniques have been demonstrated to be very powerful to understand the nanostructure evolution during dynamic processes such as electroplating,[28] nanowire[29−31] and nanocrystal[32] growth.

* Address correspondence to yicui@stanford.edu.

Received for review November 18, 2010 and accepted March 22, 2011.

Published online March 22, 2011
10.1021/nn1031356

© 2011 American Chemical Society

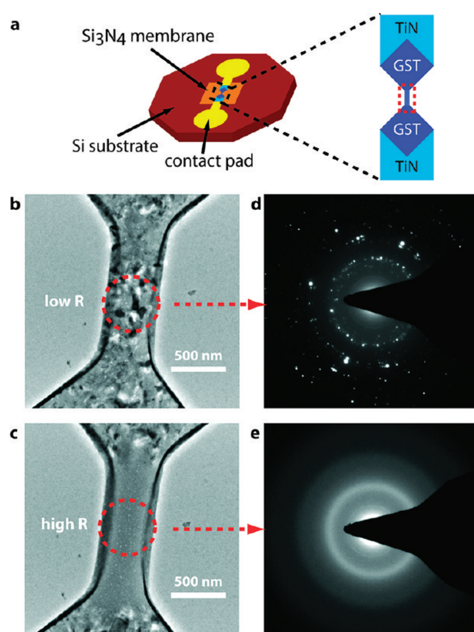

Figure 1. Device schematic and switching between crystalline and amorphous phase. (a) Schematic of silicon substrate with 50 nm silicon nitride membrane suspended at the center and GST bridge that is fabricated on the membrane. TEM image showing a bridge in the crystalline phase (b) and amorphous phase (c). The initial crystalline phase was prepared by heating the GST bridge on a hot plate at 180 °C for 10 min. The devices were capped with a 20 nm silicon oxide protective layer; therefore oxidization during heating is prevented. Typical resistance values for crystalline and amorphous phases are 10−100 kΩ and 1−8 MΩ, respectively. The red circles indicate the approximate size and location of the selected area diffraction aperture in (d) and (e). Selected area diffraction confirming the polycrystalline (d) and amorphous (e) nature of the bridge. The spot pattern acquired from the small area inside the bridge region was difficult to index, so it is unclear whether the crystal structure is face-centered cubic or hexagonal-closed packed.

We have developed a fabrication process for making single nanostructure electrical devices on TEM membranes.[33,34] In our effort to study the detailed nanostructure during repeated switching, we fabricated 50 nm thick lateral $Ge_2Sb_2Te_5$ (GST) phase-change memory bridge devices on 50 nm thick Si_3N_4 electron transparent membranes (Figure 1a), allowing us to directly correlate electrical behavior with structural changes by *in situ* TEM. These GST bridge devices were capped with a 20 nm silicon oxide protective layer to prevent oxidization of the GST film. The capping layer was deposited via atomic layer deposition. This geometry forces the current through a narrow region of GST so that sufficient heating to induce the phase change occurs in the bridge only, while the rest of the device remains crystalline at all times.

To demonstrate the feasibility of *in situ* switching, we applied short voltage pulses to devices in the crystalline state inside the TEM. The initial crystalline state was prepared by heating the GST bridge on a hot plate at 180 °C for 10 min (more information in the Supporting Information (SI), Figure 3S). Because the devices were capped with a 20 nm silicon oxide protective layer, oxidization during heating is prevented. Care was taken to avoid any influence of the electron beam on the measurement by using relatively low magnifications and spreading the beam sufficiently. Figure 1b shows an example of a crystalline bridge with typical resistances ranging from 20 to 80 kΩ. The bridge consists of a large number of micro- and nanocrystalline grains with different orientation, resulting in a granular contrast in the TEM (Figure 1b). After applying a 5 V, 400 ns square pulse with a falling edge of 20 ns, the bridge turned to an amorphous state (Figure 1c) and the resistance increased to between 0.5 and 8 MΩ. The amorphous region shows a uniform contrast in the TEM. The edge of the PCM bridge looks darker, because a thin side-wall of GST remained from the lift-off fabrication process. Switching back to the crystalline phase was accomplished by either a longer voltage pulse (2 V, 1−10 μs) or a current scan to approximately 100 μA at the ramp rate of 10 μA/s. To examine the crystallinity, we obtained selected area diffraction (SAD) of both states (Figure 1d and e), confirming the polycrystalline phase before the pulse and the amorphous phase afterward, respectively. Interestingly, applying an amorphization pulse did not always result in a pure amorphous phase as depicted in Figure 1c. Instead, about half the time we obtained an amorphous phase with nanocrystals interspersed throughout the bridge (Figures 2d and 3d), but resistances were on the order of MΩ in both cases. The SI movie 1 shows several switching cycles in real time with corresponding SAD.

To observe the details of the crystalline to amorphous transition and to measure the dependence of resistivity on the voltage pulse, we applied 400 ns pulses of varying amplitude to a crystalline device (Figure 2a). Whenever the resistance exceeded 200 kΩ, we recrystallized the device by scanning the current to 100 μA before pulsing it again. The curve shows typical PCM behavior: the general trend is that a higher pulse amplitude leads to a higher resistance, which correlates with increasing amorphization. However, we note that the resistance value depends not only on the pulse amplitude but also on the history of the sample. For example, after switching a cell from the low resistance state with the same 4 V pulse we observed a range of resulting resistance (see multiple data points at 4 V in Figure 2a).

To capture the detailed changes as we increased the pulse amplitude, we recorded TEM images of the device after consecutive 1.5, 4, and 5 V pulses (Figure 2b−d). Figure 2b shows that the bridge is predominantly crystalline with a large spread in crystal sizes. After a 4 V pulse, the resistance increased from 62 to 150 kΩ, but the change in crystallization is only minor (Figure 2b,c). After a 5 V pulse (Figure 2d), the resistance increased to

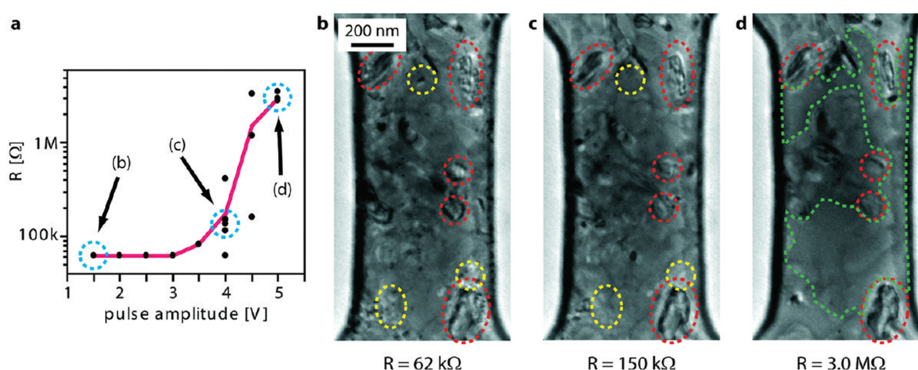

Figure 2. Study of crystalline to amorphous transition. (a) Resistance as a function of applied 400 ns voltage pulse. TEM images (b), (c), and (d) correspond to labeled points in the graph. The red line connects the average resistance values. (b–d) TEM images of phase-change memory bridge. Red ellipses show examples of crystals that survived the amorphization process. Yellow circles point out small differences in nanostructure that accompany resistance change from 62 to 150 kΩ. Green dashed lines surround areas that are predominantly amorphous.

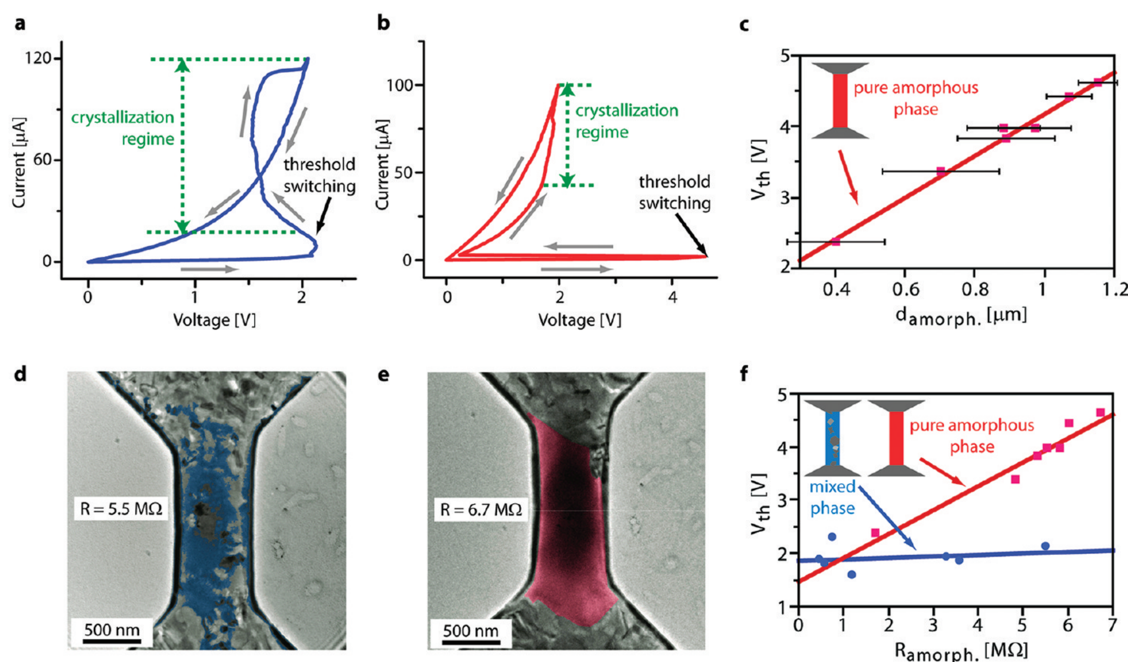

Figure 3. Measurement of threshold switching in high-resistance bridges. (a) *IV* curve showing 120 μA current scan to crystallize the bridge in (d) and to measure the threshold voltage. This bridge exhibits complicated switching behavior. (b) *IV* curve showing 100 μA current scan to crystallize the bridge in (e) and to measure the threshold voltage. This bridge exhibits clean switching behavior. (c) Threshold voltage as a function of the size of the amorphous region. The size of the amorphous region was estimated by measuring the area of the bridge that showed a uniform contrast. (d) TEM image of mixed phase bridge before current scan (a). The approximate amorphous domain has been colored blue to assist with visualization. (e) TEM image of pure amorphous phase bridge before current scan (b). The approximate amorphous domain has been colored red to assist with visualization. (f) Threshold voltage as a function of resistance in the amorphous state. We observe two different behaviors depending on the purity of the amorphous phase.

3 MΩ and a significant amorphous domain (indicated by green dashed line) interspersed with crystals was observed. The amorphous domain was estimated by measuring the area of the uniform contrast, which indicates the amorphous region. Due to strong diffraction contrast, crystallite regions appear very dark, while the amorphous region appears as uniform gray. To confirm the crystallinity of the bridge, we also obtained SAD at various resistances after switching (SI Figure S1). Evidently, resistance is not simply proportional to the size of the amorphous region, but is rather a function of the detailed crystalline and amorphous phase distribution that determines available conduction pathways. During pulsing, the larger crystals (∼100 nm) survived the melting (some examples indicated by red ellipses in Figure 2b–d). Smaller crystals (<50 nm) tended to disappear (yellow ellipses in Figure 2b,c) after the 4 V pulse, indicating that some degree of vitrification occurred. After the 5 V pulse, significant melt-quenching occurred, but the pulse was still insufficient to completely melt the larger crystals (Figure 2d, area encompassed by green line is mostly amorphous). The device

could be switched back and forth dozens of times with the same crystals remaining in the amorphous phase. The supplementary movie demonstrates the reversible switching of the device and the stable crystals that remain in the amorphous phase. The movie shows that the microstructure of the crystalline phase appears similar between switching cycles as long as the same voltage pulse is applied. However, after a longer pulse (500 ns), the larger crystals were more likely to melt completely, and in that case the amorphous domain showed only little crystalline residue even after repeated switching. These detailed observations demonstrate the value of the *in situ* TEM technique and reveal the complex relationship between voltage pulses and crystallinity as a source of the variability that is often observed in PCM measurements. Careful study of Figure 2b−d suggests that besides the pulse amplitude and time, the nanostructure of the final high-resistance state is influenced by factors such as the initial size distribution of crystals and available current paths that can lead to localized heating and melting. While the resistance of the amorphous state was always in the MΩ range, we expect that its nanostructure can have a significant impact on the electrical behavior. We note that during amorphization we did not observe any apparent volume changes in the bridge. As these devices are capped with a protection layer, it cannot be expanded in a vertical direction. Laterally, based on TEM images, there is no clear area increase. The details of the nanostructural changes during switching can be influenced by the size of the GST bridge. For smaller GST bridges, a more uniform, amorphous bridge after voltage pulses can occur due to faster and more uniform heating (SI Figure S5 shows a TEM result of a smaller bridge). A scanning EDX study did not show any clear changes in chemical compositions more than approximately 5%. However, changes lower than 5% could be possible, and more careful studies are necessary.

Since this study allows for an accurate observation of the amorphous phase, it is an ideal method to study the electric field required to induce threshold switching and to measure what effect the purity of the amorphous phase has on threshold switching. Knowing the exact threshold field is important for the design and operation of PCM cells. Especially lateral cells have shown a dramatic dependence on this parameter, because large electric fields can result in current spikes and destructive switching.[10] To measure the threshold field, we first switched the bridge to the high-resistance state, estimated the size of the amorphous region, and then performed a current scan while measuring the applied voltage to recrystallize the bridge. As expected, we observed two different behaviors in the voltage response to the current scan corresponding to different levels of purity of the amorphous phase.

If the amorphous phase is relatively pure, meaning there is very little crystalline residue inside the bridge (Figure 3e), then the *IV* curve shows a very clean snapback[3,23] once the threshold voltage is reached (Figure 3b). At this point the entire bridge is in a dynamic conductive state that is still amorphous with a current of 10 μA: too low to produce significant heating. As the current is further increased, the bridge crystallizes. The *IV* curve in Figure 3b shows that the voltage in the up-scan is close to the voltage in the down-scan, indicating that the resistance in the dynamic on-state immediately after threshold switching is very similar to the resistance after crystallization has taken place.

In contrast to the threshold switching for a pure amorphous phase, the required voltage to switch a mixed phase (Figure 3d) is much lower (Figure 3a) and the *IV* curve does not show a clean snapback. These differences in electrical behavior may be due to the complicated crystalline−amorphous mixture that can lead to conductive percolation paths when the threshold field is exceeded locally. Once such a conductive filament exists, it causes local heating and crystallization, resulting in continuously lowering the resistance of the bridge (Figure 3a). The complexity of the *IV* behavior suggests that several processes, including threshold switching, localized heating, and crystallization, may be occurring simultaneously. The exact mechanism for this *IV* curve is unclear. When switching back and forth several times, we found that the threshold voltage is nearly constant at about 2 V regardless of the resistance for a mixed amorphous phase with crystalline residue (Figure 3f). SI Figure S2 shows two more examples of threshold switching correlated with crystal structure. Direct correlation between the *IV* behavior and the detailed nanostructure of the amorphous phase using *in situ* TEM can explain the source of variability that is observed in conventional current scans. With this knowledge one may form conclusions about the crystal purity of the amorphous phase simply by studying the current scan response.

If the amorphous phase is relatively pure as shown in Figure 3e, the threshold voltage scales nearly linearly with the resistance as one would expect, because the resistance and required threshold voltage should be dominated by the smallest separation distance between the two crystalline regions at the contacts (Figure 3f). By measuring the shortest distance between crystal paths in the pure amorphous domain, d_{amorph}, and comparing it to the threshold voltage, we estimate the required threshold field to be on the order of 4 $V\cdot\mu m^{-1}$. When plotting the threshold voltage as a function of the estimated size of the amorphous domain, we obtain a near linear relationship for the pure amorphous phase (Figure 3c). Again we note that the size of the amorphous domain was estimated by measuring the area of uniform gray contrast. Since the mixed amorphous phase is interspersed with

nanocrystals and depends on percolation paths rather than the electric switching of a clearly defined region, it is not possible to measure a corresponding d_{amorph}. Interestingly, the threshold field we measured for the pure amorphous GST phase is about 1 order of magnitude below what has been reported by other groups who have investigated PCM bridges.[10,35] One factor for this discrepancy could be that small crystals (less than 10 nm), besides the ones we observe clearly, may be embedded in the amorphous phase, lowering the threshold field. These crystals would not be observed in our TEM images because the contrast from them would be small due to the thickness of the sample (50 nm SiNx TEM membrane, 50 nm GST film, and 20 nm silicon oxide capping layer) and low magnifications we worked at, which was to minimize beam damage. Also, the discrepancy may be partially due to the differences in how the amorphous phase of the GST film was prepared; here, the amorphous phase was induced by electrical pulses, instead of being as-deposited. While the origin of this disparity is still under investigation, we note that the lower threshold field was necessary for reversible switching. The groups who measured larger threshold fields found the resulting threshold voltage for $Ge_2Sb_2Te_5$ prohibitively high, as it prevented switching from the amorphous to the crystalline state.[10] This observation further corroborates the need for careful studies that can pinpoint variables that affect the threshold field.

Factors contributing to measured threshold field variability between research groups include differences in materials composition, processing, cooling rates during melt-quenching, and the difference between melt-quenched and as-deposited amorphous phases. To confirm the composition of our films, we have performed careful energy dispersive X-ray spectroscopy and diffraction analysis of the film (SI Figure S3), corroborating a composition of $Ge_2Sb_2Te_5$ within approximately 2 atomic % experimental error. Since etching can change the material properties of GST, we avoided etching and used a lift-off process instead. Similarly, we took precautions to limit exposure of the phase-change bridge to solvents. Further studies are needed to find the root cause of the variation in threshold fields. Our *in situ* technique may be a useful tool in this investigation, because it allows a direct correlation between the electrical and structural properties. A better understanding of the contributing factors may allow engineering of the material to obtain threshold fields that result in desirable threshold voltages for a given device geometry.

The above discussion shows that the nanostructure of the high-resistance state is very important for device performance. It may be that a pure amorphous phase will show less resistance drift and longer data retention due to its single-phase nature, or it could also relax faster over time, inducing more resistance drift. A longer study is necessary to answer this question. However, the mixed phase can be switched with less energy, because it requires a smaller volume to be programmed. In an effort to control the nanostructure of the amorphous phase, we manipulated the quenching rate by changing the device geometry. We created a narrower (200 nm), longer (1.5 μm), and thicker (100 nm) bridge to obtain a slower quenching rate since the main heat dissipation is through contact leads. Figure 4a shows the bridge in a low-resistance (18 kΩ) crystalline state. After applying a 2 V, 300 ns voltage pulse, the resistance increased to 176 kΩ. While the domain is still highly crystalline (Figure 4b), the disappearance of the larger crystals indicates that the complete bridge melted and then partially recrystallized due to the extended cooling time (red circles in Figure 4a,b show examples of the recrystallization). The bridge could be returned to its low-resistance state by applying a 60 μA current scan. As expected, this bridge could not be switched to a pure amorphous phase by increasing the voltage pulse (SI Figure S4). This experiment demonstrates that by changing the bridge geometry we can decrease the cooling rate and thereby increase the crystal residue of the high-resistance state. Similarly, we can achieve pure amorphous phases by using a bridge geometry with higher cooling rates (SI Figure S5). Accurate control of the cooling rates is necessary to achieve optimized switching performance.

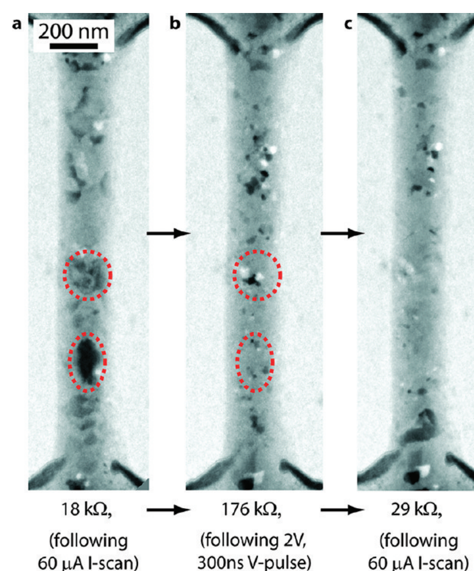

Figure 4. Switching of high-aspect-ratio bridge with lower cooling rate. (a) Crystalline bridge obtained after 60 μA current scan; resistance is 18 kΩ. The red circles show examples of large crystals embedded inside the bridge. (b) The same bridge after applying a 2 V, 300 ns pulse. The red circles show that the crystals in (a) disappeared, indicating that the bridge melted completely as a result of the pulse. However, the bridge did not turn completely amorphous but recrystallized due to the lower cooling rate. (c) The same bridge after 60 μA current scan; resistance is 29 kΩ.

In summary, *in situ* TEM studies of PCM cells during switching enable observation of the phase change

with unprecedented accuracy. Using this technique, we found significant variability in the nanostructure of the high-resistance phase, which explains the observed variability in PCM switching measurements. In particular, we observed two distinct high-resistance phases: a pure amorphous phase and a mixed amorphous phase with crystalline residues. The technique will allow further investigation of current topics in PCM such as the source of resistance drift, scaling behavior, properties of other phase-change materials, failure mechanisms, and multistate switching. In particular, energy-filtered TEM or EDX scan maps can be carried out *in situ* to investigate how the chemical composition might change. As EDX scan maps require long acquisition time, typically tens of minutes, energy-filtered TEM will be more ideal. The observations presented here as well as future studies using this technique can assist in the design of improved PCM cells.

METHODS

Device Fabrication. We used standard 50 nm low-stress silicon nitride membranes on 200 μm silicon frames as substrates. Photolithographically patterned 100 nm gold contacts were evaporated onto the substrates to allow contact to be made between the *in situ* electrical biasing holder and the PCM bridges (Figure 1a). We used electron beam lithography and a lift-off technique to pattern the TiN contacts and $Ge_2Sb_2Te_5$ cells. Both films were sputtered from stoichiometric targets in an AJA sputtering system. After lift-off, the devices were encapsulated by a 20 nm layer of sputtered SiO_2. Since the as-sputtered $Ge_2Sb_2Te_5$ layer is amorphous, we heated the completed devices on a hot plate at 180 °C for 10 min to achieve initial crystallization.

Electrical Testing and TEM Observation. The completed devices were glued with carbon paste into a custom electrical biasing holder (Hummingbird Scientific). Electrical contact was established via wire bonding between the holder and the gold pads on the substrate. We used a FEI Tecnai G2 F20 X-TWIN TEM operating at 200 kV for *in situ* observation. Pulsing and *IV* measurements were performed with a B1500A parameter analyzer (Agilent Technologies) equipped with a B1525A semiconductor pulse generator unit. For amorphization pulses, the rise and fall times were 20 ns; for crystallization pulses, the rise and fall times were 500 ns. Resistances were measured at a bias of 0.1 V. To ensure that the switching measurements were not influenced by the TEM's electron beam, we performed several control experiments in which we switched repeatedly with the column valve closed (*i.e.*, electron beam blocked by the column valve). We did not find any significant difference in switching behavior with the column valve closed or open and conclude that the electron beam plays no significant role in our measurements.

Acknowledgment. Y.C. acknowledges the support from the King Abdullah University of Science and Technology (KAUST) Investigator Award (No. KUS-I1-001-12) and from the Stanford Nonvolatile Memory Technology Research Initiative.

Supporting Information Available: Supplementary figures and a supplementary *in situ* TEM movie. This material is available free of charge *via* the Internet at http://pubs.acs.org.

REFERENCES AND NOTES

1. Ovshinsky, S. R. Reversible Electrical Switching Phenomena in Disordered Structures. *Phys. Rev. Lett.* **1968,** *21*, 1450–1453.
2. Adler, D.; Henisch, H. K.; Mott, S. N. The Mechanism of Threshold Switching in Amorphous Alloys. *Rev. Mod. Phys.* **1978,** *50*, 209–220.
3. Pirovano, A.; Lacaita, A. L.; Benvenuti, A.; Pellizzer, F.; Bez, R. Electronic Switching in Phase-Change Memories. *IEEE Trans. Electron Devices* **2004,** *51*, 452–459.
4. Yu, D.; Brittman, S.; Lee, J. S.; Falk, A. L.; Park, H. Minimum Voltage for Threshold Switching in Nanoscale Phase-Change Memory. *Nano Lett.* **2008,** *8*, 3429–3433.
5. Ielmini, D. Threshold Switching Mechanism by High-Field Energy Gain in the Hopping Transport of Chalcogenide Glasses. *Phys. Rev. B* **2008,** *78*, 035308.
6. Hamann, H. F.; O'Boyle, M.; Martin, Y. C.; Rooks, M.; Wickramasinghe, K. Ultra-High-Density Phase-Change Storage and Memory. *Nat. Mater.* **2006,** *5*, 383–387.
7. Milliron, D. J.; Raoux, S.; Shelby, R.; Jordan-Sweet, J. Solution-Phase Deposition and Nanopatterning of Gesbse Phase-Change Materials. *Nat. Mater.* **2007,** *6*, 352–356.
8. Lee, S. H.; Jung, Y.; Agarwal, R. Highly Scalable Non-Volatile and Ultra-Low Power Phase-Change Nanowire Memory. *Nat. Nanotechnol.* **2007,** *2*, 626–630.
9. Chen, Y. C.; Rettner, C. T.; Raoux, S.; Burr, G. W.; Chen, S. H.; Shelby, R. M.; Salinga, M.; Risk, W. P.; Happ, T. D.; *et al.* Ultra-Thin Phase-Change Bridge Memory Device Using Gesb. *Int. Electron Devices Meet. Tech. Dig.* **2006,** 777–780.
10. Lankhorst, M. H. R.; Ketelaars, B. W. S. M. M.; Wolters, R. A. M. Low-Cost and Nanoscale Non-Volatile Memory Concept for Future Silicon Chips. *Nat. Mater.* **2005,** *4*, 347–352.
11. Simpson, R. E.; Krbal, M.; Fons, P.; Kolobov, A. V.; Tominaga, J.; Uruga, T.; Tanida, H. Toward the Ultimate Limit of Phase Change in Ge2Sb2Te5. *Nano Lett.* **2009,** *10*, 414–419.
12. Hong, S.-H.; Bae, B.-J.; Lee, H. Fast Switching Behavior of Nanoscale $Ag_6In_5Sb_{59}Te_{30}$ Based Nanopillar Type Phase Change Memory. *Nanotechnology* **2010,** *21*, 025703.
13. Lee, S.; Jeong, J.-h.; Wu, Z.; Park, Y.-W.; Kim, W. M.; Cheong, B.-k. Demonstration of a Reliable High Speed Phase-Change Memory Using Ge-Doped SbTe. *J. Electrochem. Soc.* **2009,** *156*, H612–H615.
14. Lencer, D.; Salinga, M.; Grabowski, B.; Hickel, T.; Neugebauer, J.; Wuttig, M. A Map for Phase-Change Materials. *Nat. Mater.* **2008,** *7*, 972–977.
15. Raoux, S.; Jordan-Sweet, J. L.; Kellock, A. J. Crystallization Properties of Ultrathin Phase Change Films. *J. Appl. Phys.* **2008,** *103*, 114310.
16. Hegedus, J.; Elliott, S. R. Microscopic Origin of the Fast Crystallization Ability of Ge-Sb-Te Phase-Change Memory Materials. *Nat. Mater.* **2008,** *7*, 399–405.
17. Kolobov, A. V.; Fons, P.; Frenkel, A. I.; Ankudinov, A. L.; Tominaga, J.; Uruga, T. Understanding the Phase-Change Mechanism of Rewritable Optical Media. *Nat. Mater.* **2004,** *3*, 703–708.
18. Sun, Z. M.; Zhou, J.; Ahuja, R. Unique Melting Behavior in Phase-Change Materials for Rewritable Data Storage. *Phys. Rev. Lett.* **2007,** *98*, 055505.
19. Welnic, W.; Pamungkas, A.; Detemple, R.; Steimer, C.; Blugel, S.; Wuttig, M. Unravelling the Interplay of Local Structure and Physical Properties in Phase-Change Materials. *Nat. Mater.* **2006,** *5*, 56–62.
20. Akola, J.; Jones, R. O. Structural Phase Transitions on the Nanoscale: The Crucial Pattern in the Phase-Change Materials $Ge_2Sb_2Te_5$ and GeTe. *Phys. Rev. B* **2007,** *76*, 235201.
21. Sun, Z.; Zhou, J.; Ahuja, R. Structure of Phase Change Materials for Data Storage. *Phys. Rev. Lett.* **2006,** *96*, 055507.
22. Pirovano, A.; Lacaita, A. L.; Pellizzer, F.; Kostylev, S. A.; Benvenuti, A.; Bez, R. Low-Field Amorphous State Resistance and Threshold Voltage Drift in Chalcogenide Materials. *IEEE Trans. Electron Devices* **2004,** *51*, 714–719.
23. Ielmini, D.; Lacaita, A. L.; Mantegazza, D. Recovery and Drift Dynamics of Resistance and Threshold Voltages in

Phase-Change Memories. *IEEE Trans. Electron Devices* **2007,** *54*, 308–315.
24. Kwon, M.-H.; Lee, B.-S.; Bogle, S. N.; Nittala, L. N.; Bishop, S. G.; Abelson, J. R.; Raoux, S.; Cheong, B.-k.; Kim, K.-B. Nanometer-Scale Order in Amorphous $Ge_2Sb_2Te_5$ Analyzed by Fluctuation Electron Microscopy. *Appl. Phys. Lett.* **2007,** *90*, 021923.
25. Lee, B.-S.; Burr, G. W.; Shelby, R. M.; Raoux, S.; Rettner, C. T.; Bogle, S. N.; Darmawikarta, K.; Bishop, S. G.; Abelson, J. R. Observation of the Role of Subcritical Nuclei in Crystallization of a Glassy Solid. *Science* **2009,** *326*, 980–984.
26. Song, S. A.; Zhang, W.; Jeong, H. S.; Kim, J.-G.; Kim, Y.-J. *In Situ* Dynamic Hr-Tem and Eels Study on Phase Transitions of $Ge_2Sb_2Te_5$ Chalcogenides. *Ultramicroscopy* **2008,** *108*, 1408–1419.
27. Yoon, S.-M.; Choi, K.-J.; Lee, N.-Y.; Lee, S.-Y.; Park, Y.-S.; Yu, B.-G. Nanoscale Observations of the Operational Failure for Phase-Change-Type Nonvolatile Memory Devices Using $Ge_2Sb_2Te_5$ Chalcogenide Thin Films. *Appl. Surf. Sci.* **2007,** *254*, 316–320.
28. Williamson, M. J.; Tromp, R. M.; Vereecken, P. M.; Hull, R.; Ross, F. M. Dynamic Microscopy of Nanoscale Cluster Growth at the Solid-Liquid Interface. *Nat. Mater.* **2003,** *2*, 532–536.
29. Kodambaka, S.; Tersoff, J.; Reuter, M. C.; Ross, F. M. Germanium Nanowire Growth below the Eutectic Temperature. *Science* **2007,** *316*, 729–732.
30. Stach, E. A.; Pauzauskie, P. J.; Kuykendall, T.; Goldberger, J.; He, R.; Yang, P. Watching Gan Nanowires Grow. *Nano Lett.* **2003,** *3*, 867–869.
31. Wen, C. Y.; Reuter, M. C.; Bruley, J.; Tersoff, J.; Kodambaka, S.; Stach, E. A.; Ross, F. M. Formation of Compositionally Abrupt Axial Heterojunctions in Silicon-Germanium Nanowires. *Science* **2009,** *326*, 1247–1250.
32. Zheng, H.; Smith, R. K.; Jun, Y.-w.; Kisielowski, C.; Dahmen, U.; Alivisatos, A. P. Observation of Single Colloidal Platinum Nanocrystal Growth Trajectories. *Science* **2009,** *324*, 1309–1312.
33. Peng, H. L.; Xie, C.; Schoen, D. T.; Cui, Y. Large Anisotropy of Electrical Properties in Layer-Structured In_2Se_3 Nanowires. *Nano Lett.* **2008,** *8*, 1511–1516.
34. Meister, S.; Schoen, D. T.; Topinka, M. A.; Minor, A. M.; Cui, Y. Void Formation Induced Electrical Switching in Phase-Change Nanowires. *Nano Lett.* **2008,** *8*, 4562–4567.
35. Krebs, D.; Raoux, S.; Rettner, C. T.; Burr, G. W.; Salinga, M.; Wuttig, M. Threshold Field of Phase Change Memory Materials Measured Using Phase Change Bridge Devices. *Appl. Phys. Lett.* **2009,** *95*, 082101.